Journal of Applied Polymer Science

Silica-based self-healing microcapsules for self-repair in concrete

Noel Peter Bengzon Tan, Lok Hang Keung, Wing Ho Choi, Wai Chak Lam, Hei Nga Leung
Nano and Advanced Materials Institute, Ltd. (NAMI), Units 608-609, 6/F, Lakeside 2, No. 10 Science Park West Avenue, Hong Kong Science Park, Shatin New Territories, Hong Kong
Correspondence to: L. H. Keung (E-mail: rogerkeung@nami.org.hk); N. P. B. Tan (E-mail: bengzontan@nami.org.hk)

ABSTRACT: New self-healing material for concrete repair has been fabricated through microencapsulation of silica sol via interfacial polymerization of poly(urea-urethane). Smooth, uniform, and spherical capsules of 60–120 μm sizes were synthesized and optimized by studying the emulsification and polymerization steps of its synthesis. A hydrophile–lyophile balance (HLB) value of 3.0–5.0 and a rotational speed of 500 rpm were necessary to produce a stable emulsion system of silica sol in surfactants. The polymerization speed of 900 rpm and the methylene diisocyanate (MDI) monomer content of 15 wt % were both significant in getting the right size and smoothness of the microcapsules. With this method and cheap healing agents, industrial scale-up is highly possible. The viscoelastic properties of the microcapsules were examined, and further characterizations were carried out through scanning electron microscopy, energy dispersive X-ray spectroscopy, and Fourier transform infrared spectroscopy. After healing the microcracks in concrete, the results showed that the significant increase of compressive and bending strengths manifested the self-healing ability of the microcapsules in concrete. © 2015 Wiley Periodicals, Inc. J. Appl. Polym. Sci. **2016**, *133*, 43090.

KEYWORDS: applications; characterization; polyurethanes; properties

Received 26 June 2015; accepted 26 October 2015
DOI: 10.1002/app.43090

INTRODUCTION

For the past decade, research on self-healing materials has gained increased attention since its fundamental conception, as carried out by the group of White *et al.*[1] Self-healing material can repair itself when damaged or when degradation occurs. Its concept was inspired by a biological point of view of self-repairing tissues in plants, microorganisms, and humans. The goal of self-healing material is to extend the service lifetime of structures and systems made with them.[2]

One of the prominent emerging applications of self-healing materials is in building and construction, such as concrete. Concrete is cheap and the most common structural material used in buildings, bridges, and tunnels. Preventive measures for concrete degradation, such as inspection and maintenance, are key activities carried out to lengthen its life and monitor its conditions. However, concrete is prone to crack, and if not treated promptly, degradation and collapse of the structure is inevitable. Therefore, immediate response to concrete degradation at the micro level is of high importance. One way to address this is by incorporating self-healing materials into the concrete.

Several studies have been carried out using self-healing materials in concrete. For example, Li *et al.*[3] were able to study passive self-healing cementitious composites. The group used hollow, brittle glass fibers with superglue (i.e., ethyl cyanoacrylate) as the healing agent. The glass fiber with the superglue was partially embedded in an engineered cementitious composite (ECC) specimen loaded in a controlled manner. Once overloaded, tensile cracking of the specimen occurred and broke the glass fiber. As the glass fiber broke, a healing agent was released into the cracks of the cementitious matrix and healed it. Pang and Bond studied another developed hollow fiber.[4] They produced a container with a large internal volume to maximize the storage capacity of the healing agent (a dilute epoxy resin). The fabricated composite was used to study the biomimetic approach to demonstrate its self-repair mechanism by incorporating UV-fluorescent dye into the composite. A similar device was also created by the group of Nishiwaki *et al.*[5] The group used a self-diagnosing composite, made of an organic pipe film containing the healing agent (a low-viscosity epoxy resin) and a heating device. The self-diagnosing composite is embedded into concrete to self-heal when a crack is generated. When a crack is made, the heating device warms the crack and eventually melts the surface of the organic film, releasing the healing agent. The healing agent fills up the crack and hardens it. Unfortunately, these types of self-healing systems are not applicable for large-scale industries, considering their short shelf life and the high cost of healing agents.

Another type of self-healing agent in concrete is the use of microorganisms. A certain strain of bacteria can be used as a

medium for the precipitation of salts, healing the cracks within the concrete. The most common type of precipitation by bacteria is of calcium carbonate ($CaCO_3$) and polymorphic iron aluminum silicate, $(Fe_5Al_3)(SiAl)O_{10}(OH)_5$. Different approaches are used to incorporate the microorganism into the concrete. Some microbial broths are directly mixed into the fresh concrete, while others are in the form of spores, capsules, gels, and vascular networks.[6–8] The selection of bacteria depends on its survival capability in an alkaline environment (pH 10–13), temperatures that can go as high as 70°C, and a limitation of water. Strains of bacteria genus *Bacillus* are used to overcome the highly alkaline environment in concrete. For example, *Bacillus pasteurii* immobilized in polyurethane[9] was used to produce enzymes for hydrolysis of urea, inducing calcite ($CaCO_3$) precipitation. Calcite exhibits a filling potential for concrete cracks and fissures, eventually overcoming environmental degradation for an extended period. Jonkers *et al.*[10] were also able to directly incorporate alkali-resistant, spore-forming bacteria *(B. pseudofirmus* and *B. cohnii*) and calcium lactate as two-component self-healing agents of cement paste. These bacteria were able to produce the abundant amount of minerals needed to fill or seal formed cracks. The same effect was found in other types of bacteria used in concrete, such as *B. lintus*,[11] and *B. sphaericus*.[12] Apparently, ureolytic bacteria are one of the most popular ways to design self-healing concrete.[13] This type of bacteria produces extracellular urease enzyme, which fastens the series of biochemical reactions involved in the formation of calcium carbonate. A similar proof of concept of crack remediation on structures was demonstrated by the group of Rodriquez-Navarro *et al.*[14] The group was able to produce *Myxococcus xanthus*-induced calcium carbonate precipitation that protects and consolidates porous ornamental limestone (e.g., monuments and statuary). To overcome the high temperature within the concrete mix, a thermophilic anaerobic microorganism *(Shewanella*) was also incorporated in the cement mortar.[15] The results revealed that the comprehensive strength of the concrete increased. This improvement was due to the deposition of microorganism cell surfaces within pores of the cement-sand matrix. However, microbiologically induced calcite precipitation mainly occurred on the surface of the concrete crack. Also, the polyurethane immobilized in this process also generates carbon dioxide, which can be detrimental to the microorganism. As a result, enzyme activity from the microorganism decreases and prohibits the calcite precipitation. Another drawback of this method is the production of ammonium ions, which results in excessive nitrogen loading. There is also the loss of viability of bacterial pores that results in decreased mineral-forming capacity. Therefore, its application is limited to young concrete.

A not-as-famous biological precipitation reaction assisted by *Leuconostoc mesenteroides* is polymorphic iron aluminum silicate.[16] This bacterium produces lactic acid from carbohydrate, resulting in an acidic environment, while the reduced solubility of colloidal silica results in precipitation. However, because of its acidic nature, this method may not be useful for the durability of concrete. Another source of microorganism-driven self-healing mechanism in concrete is the use of fungi. Although it is not yet clearly understood how fungi-assisted precipitation can fill cracks in concrete, it can be a good research area to pursue.[17]

Most recently, self-healing materials applied on a polymer matrix were developed by the group of White *et al.*[18] This type of material is in the form of microcapsules that contain a healing agent (e.g., dicyclopentadiene). Healing agents were microencapsulated with poly(urea-formaldehyde) through in situ polymerization. In their study, the microcapsules, together with Grubbs' catalyst, were embedded in a polymer matrix. Microcapsules break through crack propagation and then release the healing agent into the crack plane through capillary action. Polymerization of the healing agent occurs during contact with the catalyst, resulting in the bonding of the cracks. The group of Hu *et al.* adopted a similar approach to producing microcapsules.[19] The use of melamine formaldehyde (MF) as a protective shell layer for the healing agent makes a stronger microcapsule and ruptures at large deformations. These microcapsules provide a bigger scope of formulation and processing conditions to manipulate, which is desirable for self-healing applications. A much higher efficiency of microcapsule healing was developed by Li *et al.*,[20] in which polyetheramine was used as the healing agent and poly(methyl methacrylate) (PMMA) was used as the encapsulating shell. Polyetheramine was chosen as a curing agent because of its flowability and low-temperature curability. PMMA was selected as a shell because of its chemical stability, biocompatibility, and compatibility with epoxy. The solvent evaporation method was used to form a polymeric shell around the reactive amine of the polyetheramine core. However, the cost of these healing agents is relatively high, and some may cause environmental and health hazards. To address this problem, the group of Huang *et al.* developed a water-based healing material [$Ca(OH)_2$] microcapsules.[21] Unfortunately, this type of microcapsule gives a very low healing efficiency, due to the absorption of the healing agent into the bulk matrix.

Among the three systems of self-healing in concrete reviewed previously, microcapsules seem to be the most practical for industrial commercialization. The primary driver of this study is to create microcapsules that can be industrially scaled up for concrete application. One way to initialize the scalability of microcapsules is to find innovative alternatives for healing agents. Based on our preliminary investigation of using silica sol ($SiO_2{\cdot}H_2O$) as a healing agent, it was found that this type of colloidal system could fill cracks in concrete. A similar system was first introduced by Pelletier *et al.*,[22] who used sodium silicate stored in polyurethane microcapsules as a self-healing agent in concrete. The sodium silicate is released when the capsules are ruptured by propagating cracks and react with the calcium hydroxide [$Ca(OH)_2$] present in the cement, which then produces C–S–H [$(CaO\ SiO_2)\ H_2O$] gel that heals the cracks. Kendrick *et al.*[23] further studied the reaction of microsilica to calcium hydroxide and confirmed the formation of C–S–H. Different types of SiO_2 (e.g., amorphous and crystalline) were investigated by Baltakys *et al.*[24] by reacting them with calcium hydroxide. It was found that the phase composition and properties of calcium silicate hydrates (C–S–H) were strongly affected by the crystallinity of SiO_2. It was also concluded that the entire

reaction of C–S–H is observed sooner in the amorphous than in the crystalline form of SiO_2.

Despite the numerous studies of silica forming C–S–H gel as filler for cement cracks, to the best of our knowledge no one has yet created silica microcapsules as a self-healing agent in concrete. This study focuses on the synthesis of a silica-based core material as self-healing microcapsules for concrete strength recovery. In this study, colloidal silica was used as the healing agent instead of any other forms (e.g., sodium silicate). The use of this is due to its amorphous nature, low viscosity, and high amounts of SiO_2 responsible in the formation of gels. It is cheap, commercially available, and, with existing technology for secure microencapsulation, commercialization is highly possible shortly.

In this study, interfacial polymerization was used to form microcapsules with silica sol as the core and a polymeric shell coating. Saihi *et al.* have performed this type of synthesis[25] in microencapsulating ammonium phosphate with a polyurethane shell. This technique was chosen because of its very straightforward approach and the way it can be accomplished in just a one-step process. With cheap materials and very easy synthesis, an industrial scale is possible in this technique. In a very recent review on self-healing polymeric materials based on a microencapsulated healing agent,[45] it was stated that this type of approach is more likely to be commercialized in the near future for the following reasons: (1) no changes in the molecular structure are required to integrate the polymers with self-healing abilities, (2) microencapsulation has matured as a technology since its emergence in the 1950s, and (3) healing-agent-loaded microcapsules can be readily incorporated into the polymer matrix using blending techniques. The group further recommends that continuous efforts be devoted to this research to facilitate a large-scale application of self-healing materials. In fact, a pilot-scale plant of a 10 L capacity batch reactor was successfully installed.

In this study, we propose the use of a procedure based on interfacial polymerization to synthesize self-healing microcapsules from aqueous silica. A nonprovisional US patent pending has been filed related to this study.[26] The objectives of this work are to optimize microcapsules by investigating the influence of the hydrophile–lyophile balance (HLB) value based on the surfactant ratios and to study the effects of emulsification, polymerization speed, and monomer ratios applied during the polymerization stage. It was found that in order to attain the optimized self-healing microcapsules for applications in concrete repair, an HLB value of 3–5 was necessary to attain the most stable emulsion system, with emulsification speed of 500 rpm and polymerization speed of 900 rpm. The smoothness of microcapsules is further achieved at a polymerization speed of 700–1100 rpm. However, in this case, 900 rpm was used in most experiments.

The potential application of silica sol as a healing agent was initially investigated in both foam and ordinary concretes. The characterization of the self-healing microcapsules was carried out by scanning electron microscopy (SEM), energy dispersive X-ray spectroscopy (EDS), Fourier transform infrared spectroscopy (FTIR), nanoindentation, and a dynamic mechanical analyzer.

EXPERIMENTAL

Materials

Colloidal silica (LUDOX TM-50, 50 wt % suspension in H_2O) as core material, with Span 85 (sorbitane trioleate) and poly(ethylene glycol) dioleate (POEDO) as surfactants, along with 4,4′-methylenebis(phenyl isocyanate) 98% (MDI) as shell-forming monomer and dibutyltin dilaurate 95% (DBTL) as catalyst, were all purchased from Sigma-Aldrich (St. Louis, MO, USA). Toluene was a reagent grade purchased from Macron Fine Chemicals Avantor Performance Materials (Center Valley, PA, USA) and used without further purification. Superplasticizer (MasterGlenium SKY 8588) was purchased from BASF (Ludwigshafen, Germany).

Synthesis of Silica-Based Self-Healing Microcapsules

The preparation of self-healing microcapsules containing silica sol was performed in a 100 mL beaker with a magnetic cylindrical stirrer bar by interfacial polymerization, according to the adopted method.[27] In a typical experiment, 30 mL of aqueous colloidal silica (50% w/w) was emulsified in an organic phase containing toluene (64 mL) and 5 wt % binary mixture of POEDO and Span 85 at a speed in the range 50–12,000 rpm. After 10 min of emulsification, polymerization was accomplished with the addition of a solution containing a fixed amount of monomer (1–15 wt % of MDI) in toluene, at 63°C for 90 min in the speed range 300–1000 rpm. This process formed a polymeric crosslinked shell, encapsulating the silica core material, with two drops of catalyst, DBTL. The microcapsules produced were then washed with toluene to remove the remaining MDI residue.

Microencapsulation yields (% Y) were calculated based on the microcapsules produced over the total amount of introduced MDI monomer, surfactants, and silica sol. The % Y is calculated by the formula below:

$$\%\ Y = \frac{\text{wt. of microcapsules}}{\text{wt. of silica sol} + \text{wt. of MDI} + \text{wt. of surfactants}} \times 100$$

However, encapsulation efficiency (% E) was calculated based on the molecular weight of silica sol and percent silica from EDS analysis over the molecular weight of silica:

$$\%\ E = \frac{\text{MW of silica sol} \times \%\ \text{silica}}{\text{MW of silica}}$$

Characterization of Microcapsules

FTIR spectroscopy was performed in an FTIR spectrophotometer (Bio-Rad FTS6000. Bio-Rad (Philadelphia, PA, USA)). A sample was prepared by drying and mixing with KBr salt, pressed into a disk, and measured with a spectral range of 400–4000 cm^{-1}.

SEM samples were examined in JEOL (Peabody, MA, USA)-JSM 6390 and 6300 models of a field emission scanning electron microscope at an accelerating voltage of 15–20 kV. The samples were then spread onto a copper substrate followed by air drying. A thin layer of gold film was sputtered onto the dried sample under vacuum.

EDS analyses were taken from the same SEM samples using an X-max Oxford Instruments (Abingdon, Oxfordshire, UK)

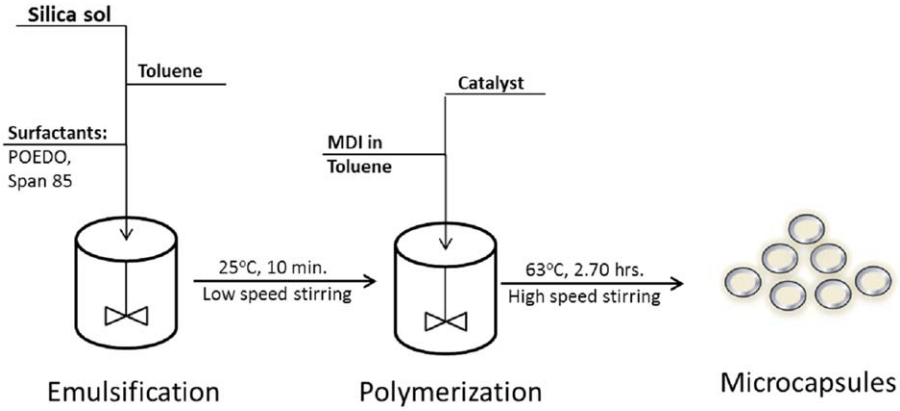

Scheme 1. Schematic representation of the synthesis of silica-based microcapsules as self-healing agent. [Color figure can be viewed in the online issue, which is available at wileyonlinelibrary.com.]

80 mm^2 model employing a mapping function. Images were taken with an optical microscope (Optika (Ponteranica, Italy) Microscopes, Italy, 100V–200V/75 VA/50/60 Hz) equipped with a Nikon (Bangkok, Thailand) digital camera (D5200).

The nanoindentation analysis was performed with a Nano Test Vantage Machine (Micro Materials (Wrexham, UK) Ltd.) with a load up to 18 mN and at a depth of 12,000 nm. The cone tip radius used was a Berkovich type. The maximum load was set to 400 mN, with loading and unloading rates for both at 5 mN/s. The dwell period at maximum load was set at 1 s.

A dynamic mechanical analyzer [DMA 7, PerkinElmer (Waltham, MA, USA)] was used to characterize the mechanical properties of the polymeric shell component of the silica-based microcapsules. The testing was carried out at room temperature with a linear force of 8000 mN on a poly(urea-urethane) film using a probe tip.

Water Absorptivity and Compressive and Flexural Tests on Concrete

The water absorptivity procedure was adapted from ASTM C642-06 and BS 1881: Part 122 for samples with 10 cm × 10 cm × 10 cm dimensions. The initial water absorptivity of the self-healing concrete and control were determined. Samples were first cured in a drying oven for 72 hours and then cooled for 24 hours at room temperature. The samples were weighed and immediately immersed in a water tank. The samples were removed from the tank after 30 min, surface dried, and weighed again. The results of the water absorptivity were an average of three replicates.

The compressive strength of self-healing concrete containing microcapsules was compared with normal concrete (control) before and after microcracking occurred. The compressive strength procedure was adapted from ASTM C39/C39M-10 and BS 1881: Part 116f for cube samples with 10 cm × 10 cm × 10 cm dimensions. The testing machine was equipped with steel bearing plates with faces larger than the size of the samples. The rate of load, or stress, ranged from 0.2 to 0.4 MPa/s. The initial compressive stresses were determined with three replicates by applying stress on samples until they reached failure. Succeeding experiments of replicates of three were performed.

The flexural strength procedure was adapted from ASTM C78/C78M-10 and BS 1881: Part 118 with samples of dimensions 22.5 cm × 7.5 cm × 3.5 cm. Each sample was subjected to an applied load of 0.50 mm/s in a four-point bending instrument. The initial strength was determined by applying the load until the sample reached failure.

The self-healing process was performed as follows: induce microcracking of samples by loading up to 80% of its strength and sustaining for 10 s, then heal cracks by submerging them in water for 3 days. After healing, the compressive and flexural strengths were retested to failure again. For the control samples, microcracking occurs at the start of loading the concrete. Therefore, loading the samples at 80% of its strength is enough to produce microcracks within the concrete.

Water content is also an issue for self-healing in concrete. However, the current technology was developed for applications in a Hong Kong environment and in other countries that have similar climate conditions. Hong Kong has a favorable amount of rainfall coupled with high relative humidity for self-healing to happen. For the past 60 years, above 2000 mm rainfall was recorded every year with a rising trend since the 1940s, resulting in an average rainfall of 38 mm/decade.[46] This is also in synergy with the high relative humidity (RH) in Hong Kong, which reaches 65–85%. At 75% RH, moisture of 2% in concrete is expected.[47] Therefore, these two factors are important to sustain water in concrete and thus to simultaneously self-heal while microcracking.

Concrete Formulation and Casting

The self-healing concrete was prepared by thoroughly mixing the concrete components and healing agent in a cement mixer. The concrete component is composed of cement, sand, crushed rock, and water in a weight ratio of 1:1.5:2:0.35, respectively. The healing-agent components were composed of plasticizers and microcapsules in a volume ratio of 0.5:1. The plasticizer was 1.5 wt % of the total weight of the self-healing concrete, and the microcapsules were 5% of the total volume of the self-healing concrete.

RESULTS AND DISCUSSION

Synthesis of Self-Healing Microcapsules

The synthesis of silica-based microcapsules was carried out in a two-step process, as shown in Scheme 1. The first step is the emulsification of silica sol with surfactants, followed by

Table I. HLB Values of Different Mixtures of Surfactant and Its Corresponding Emulsion Behavior

Emulsion stability	S	G	E	G	P	VP	VP
Silica sol (50 wt %) (mL)	30	30	30	30	30	30	30
Surfactant + toluene (mL)	70	70	70	70	70	70	70
POEDO (g)	0	1.11	2.03	2.95	3.88	4.8	6
Span 85 (g)	6	4.89	3.97	3.05	2.12	1.2	0
HLB	1.80	3.00	4.00	5.00	6.00	7.00	8.30

Emulsion classification: S, satisfactory; G, good; E, excellent; P, poor (coalescence); VP, very poor (sedimentation).

interfacial polymerization, resulting in microcapsules. Emulsification is carried out to make sure the self-healing agent, silica sol, is dispersed effectively in the organic medium using the surfactants (POEDO and Span 85). This step initially determines the size and size distribution of the microcapsules. The entire process was performed at room temperature, at low speed, and in a short period. The second step is a catalytic interfacial polymerization, which forms the polymeric shell around the predispersed silica sol. During this process, the predispersed silica is coated with poly(urea-urethane) as a result of the interaction between the MDI monomer and the surfactants' functional moieties, such as alcohol and amine. The polymerization speed is higher than emulsification. This is necessary to control the final size of the microcapsules and their mechanical strength. The microcapsules produced were monodispersed and uniform, with a core-and-shell structure. The polymeric shell layer structure is necessary to protect the core material from leaking out and for effective application in concrete.

Emulsification Step

As a first step in the microencapsulation process, it is important to optimize fully the most effective emulsification conditions of silica sol with the surfactants used. Investigating the hydrophilic–lyophilic balance properties of the surfactants with the silica sol helped accomplish this task. The goal in this approach is to find a balance of the surfactant mix favorable to the dispersion of silica sol. The balance of the surfactant mix is based on the hydrophile–lyophile balance (HLB) property concept[27] of the mixed surfactants (POEDO and Span 85). The HLB of surfactants is related to their solubility. A low HLB value indicates that the system is oil-soluble, whereas a high HLB value tends to indicate a water-soluble system. Different weight ratios of surfactants were used to come up with a different range of HLB values from 1.80 to 8.30 (see Table I). In all experiments, 30% by volume of silica sol was used and mixed for 20 min. The stability of the resulting emulsion was judged on its appearance and by observing the phase separation by the naked eye and optical microscopy. The results in Table I show that an HLB of 3.0 to 5.0 results in a good to excellent emulsion stability, while 1.8 is satisfactory. However, at higher HLB, such as a 6.0 to 8.3 mixture, the result shows a poor and unstable emulsion with coalescence and sedimentation observed. Therefore, an HLB of 3.0 to 5.0 would best be used for this mixture of surfactant with silica sol as the core material.

Formation of Poly(urea-urethane) Microcapsules through Interfacial Polymerization

Having investigated the optimum emulsification condition, the formation of the polymeric shell coating is also critical as the final step. In this step, interfacial polymerization created a polymeric shell [poly(urea-urethane)] surrounding the core material. Several studies have shown interfacial polymerization in an organic medium.[28,29] The reaction mechanism is similar, as described in the work of Salaun *et al.*[30] In this case, the mechanism involves polycondensation of diisocyanate from the MDI monomer at the interface of the emulsion droplet produced in the first stage. MDI monomers are first hydrolyzed, producing unstable amino groups. Unstable amino groups further dissociate into amine groups and carbon dioxide. The amine-functionalized MDI monomer further reacts with other MDI molecules, forming poly(urea) chains. However, other MDI molecules react with diol molecules from surfactants (Span 85) to form polyurethane chains. Therefore, the simultaneous reactions of MDI with amine and diol functional groups, occurring within the surface of emulsion droplets, result in the formation of the poly(urea-urethane) shell.

Optimization of Microcapsule Size

One of the critical parameters in synthesizing microcapsules is their size or diameter. In the application of microcapsules in concrete, the diameter is important in relation to its mechanical strength. Too-small microcapsules are hard to break, whereas too-large microcapsules are easy to crack. Therefore, getting the right microcapsule size is of great significance to its application. At an optimum size, self-healing microcapsules are hard enough not to break, yet easy enough to rupture when microcracking occurs. In this study, a target size range of 100–200 microns is obtained.

Three important parameters were investigated to optimize the silica-based self-healing microcapsules for application in concrete. These were emulsification speed, monomer ratio, and polymerization speed.

To ensure the stability of the silica sol as the core material in microcapsules, an optimum emulsification speed must be determined. In this study, eight different emulsification speeds were tested in the range of 50–12,000 rpm. After emulsification of 10 min, a drop of the sample was examined in an optical microscope. For each emulsification speed, an optical image is observed, as shown in Figure 1. It was determined that at higher speeds (e.g., 1000–12,000 rpm), silica sols formed very fine white droplets. Later, the entire mixture separated into phases.

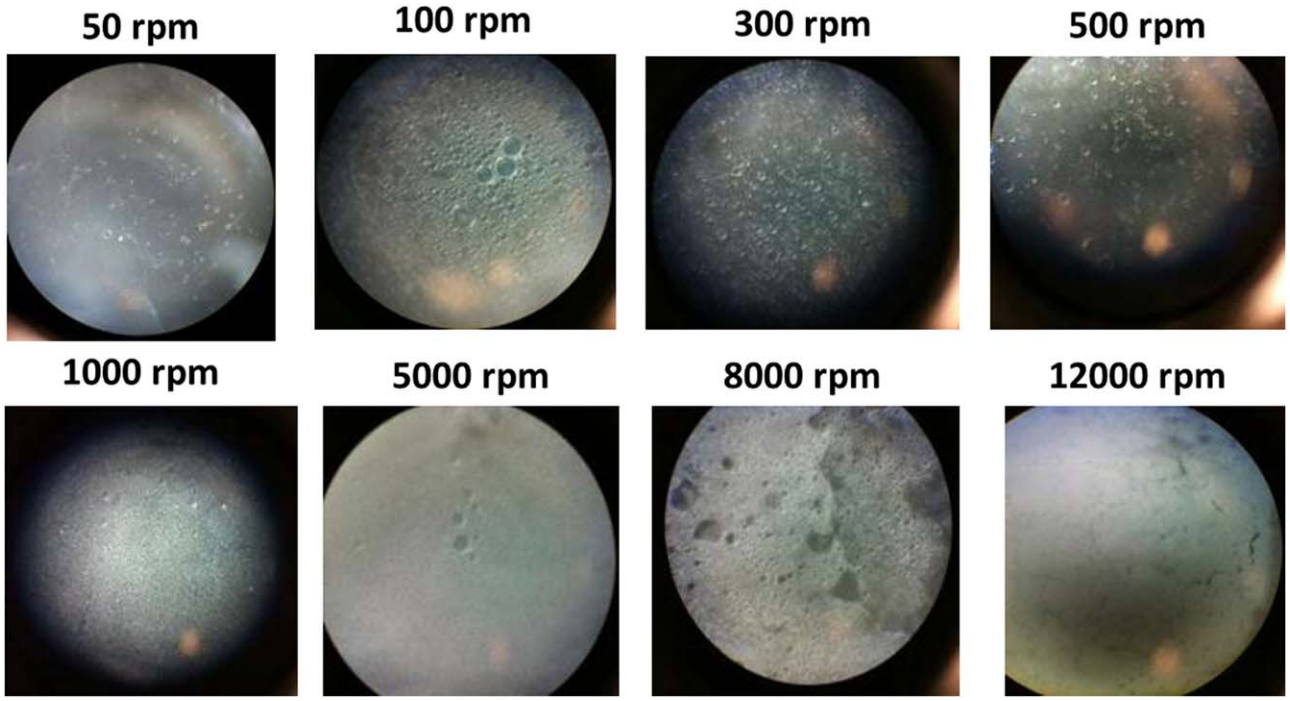

Figure 1. Optical images of emulsified silica sol with surfactants at different emulsification speeds. [Color figure can be viewed in the online issue, which is available at wileyonlinelibrary.com.]

This phenomenon was due to the increasing shear stresses that silica sol droplets underwent during emulsification. Therefore, the system was not stable, and precipitation occurred. However, at lower speeds (50–500 rpm), the corresponding optical images show dispersed silica sol droplets. This shows that a lower speed of emulsification results in more stable and dispersed silica sol droplets using the specified surfactants. In this case, 300–500 rpm was chosen to have the best conditions.

Further studies were performed by investigating the yield and encapsulation efficiencies (Figure 2) at different emulsification speeds. The results show that, in all speeds tested, their corresponding yields have no significant change, which is limited to about 30%. However, there is a change in encapsulation efficiencies. Lower speeds of 50–400 rpm give low encapsulations of about 15%, whereas 600 and 800 rpm give encapsulations as high as 65%. This means that more silica sol is encapsulated in the microcapsules during a high emulsification speed. The low encapsulation of silica sol can be attributed to the diffusion of silica sol from the droplet during emulsification. This also shows that, at low emulsification, there is not enough interaction of surfactant with silica sol to hold the silica sol within the droplet.

After knowing the optimum emulsification speed for synthesizing silica sol droplets, the polymerization speed or shell-formation rate was also investigated. The polymerization speed is critical in the microcapsule synthesis because of its strong influence on the morphology of microcapsules, such as size and porosity of the shell. Therefore, it is necessary to study the shell formation through the polymerization speed conditions and to control the shape and morphology of the microcapsules.[31,32]

The effect of polymerization speed on the size of microcapsules is depicted in Figure 3. Increasing polymerization speed decreases the average size of microcapsules. This result is consistent with the report on dicyclopentadiene (DCPD) microcapsules with poly(urea-formaldehyde) shell coating.[33] At 300 rpm, the particle size is 820 μm, and it was reduced abruptly when the speed was increased to 500 rpm. A gradual decrease in size was observed from 500 rpm up to 1000 rpm of speed, which results in 230 to 94 μm. Based on these data, the 100–200 μm target of microcapsule size is attainable at 900 rpm, giving an average of 143 μm. This suggests that polymerization speed controls the equilibrium between shear forces and interfacial

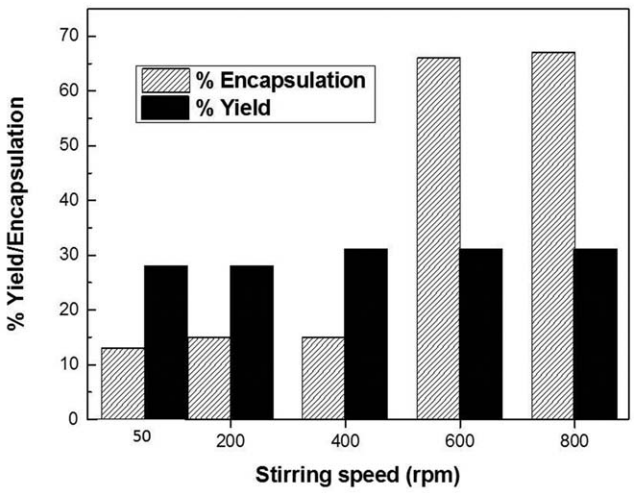

Figure 2. Yield and encapsulation efficiencies of silica sol microcapsules in different emulsification speeds.

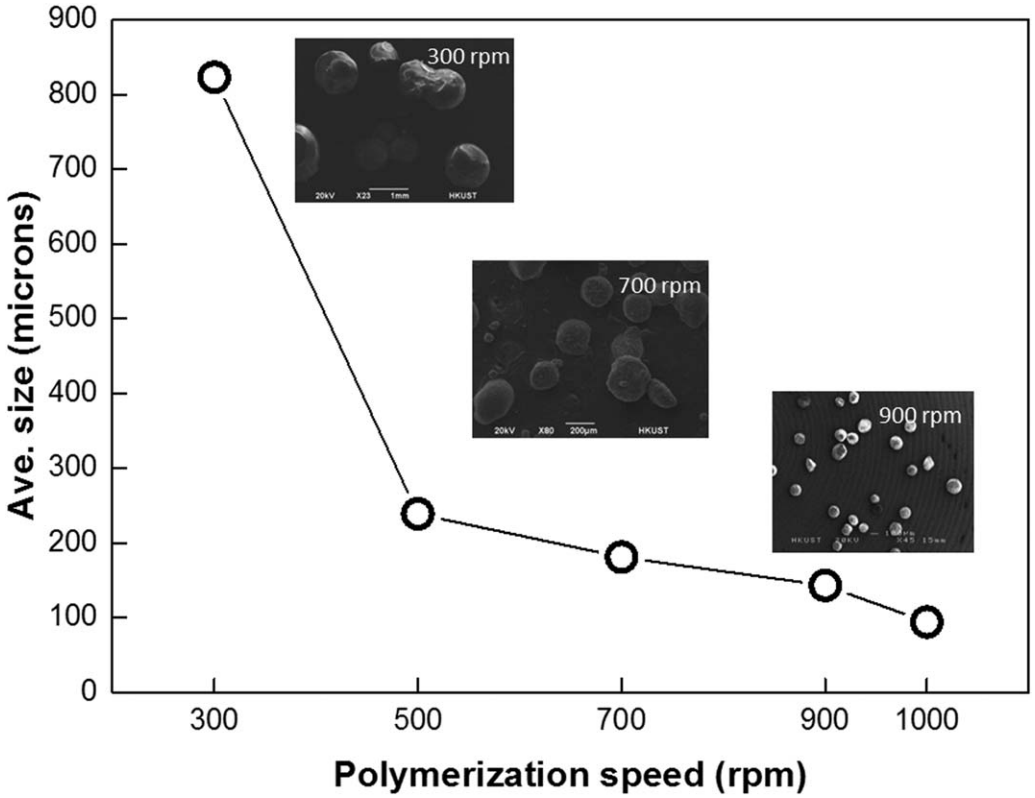

Figure 3. Effect of polymerization speed on the particle size of silica-based self-healing microparticles.

tension of the silica sol droplets and the local velocity gradient that the droplets experience.[34] This means that, at low speed, interfacial tension is higher than shear force and, therefore, produces large capsules. However, large capsules are broken into small ones when strong shear forces are higher under high speed. It was also observed at low speed that microcapsules were not uniform in size. However, as the speed increases, microcapsules become more uniform in size and shape (Figure 3, SEM inset). Such an observation can be shown by its reaction kinetics and the diffusion of diol molecules. At low speed, homogenous reaction kinetics and diffusion of diol molecules cause a nonuniform size and shell thickness, whereas, at higher speed, the interfacial area is increased, and the most homogenous reaction occurs.[35]

Aside from the obvious effects of polymerization speed on the microcapsule size, the smoothness of the shell layer or coating was also investigated (Figure 4). Smoothness is critical in preventing leakage of the core materials from the shell coating layer. This parameter is also controlled by the polymerization speed. When the polymerization speed was increased from 300 rpm to 1100 rpm, the microcapsules evolved from a very porous to a smooth surface. Large pores are observed at 300 rpm and were reduced to smaller pores when the speed was increased to 500 rpm. When speeds reached 700 rpm, the particles gradually became smoother, and the same smoothness was observed at 1100 rpm. This observation is attributed to the fact that a higher agitation rate reduces the conglomeration of poly(urea-urethane) shell formation or the polymer deposition on the droplet surface.[30] Another reason for this phenomenon is the ability of the microcapsules to form longer chains of polymeric shell coating using MDI and the surfactants. Although this was not clearly investigated, a similar phenomenon was observed in the work of K. Hong and S. Park.[33]

Clearly the result reveals that polymerization speed has a strong influence on the structure of microcapsules and that it can be controlled. It is ideal that the microcapsules produced do not possess pores, to prevent leaking of the core material, silica sol. In this case, it is best to use a polymerization speed of 700–1100 rpm, but more preferably at 900 rpm.

At constant emulsification and polymerization conditions, addition of monomer during shell formation was also investigated. This study was crucial in determining the optimum core-to-shell thickness ratio. Figure 5 shows the relationship between the percentage of weight of monomer used (MDI) with the core and the shell thickness ratio based on SEM images. A high core-to-shell ratio means that a high amount of core material (silica sol) is present in the microcapsule with a thin shell layer. The results show that the core-to-shell thickness ratio decreases as the weight of MDI monomer increases. This means that the increased addition of monomer results in a thicker shell layer. Yields are also compared, as shown in Figure 5 inset. There is an increase in yield with an increase in monomer used. However, the 15 wt % monomer gives the highest value with a minimum core-to-shell ratio. This means at this condition that the shell is at its thickest possible. Conversely, encapsulation efficiency has no significant effect on all monomer conditions.

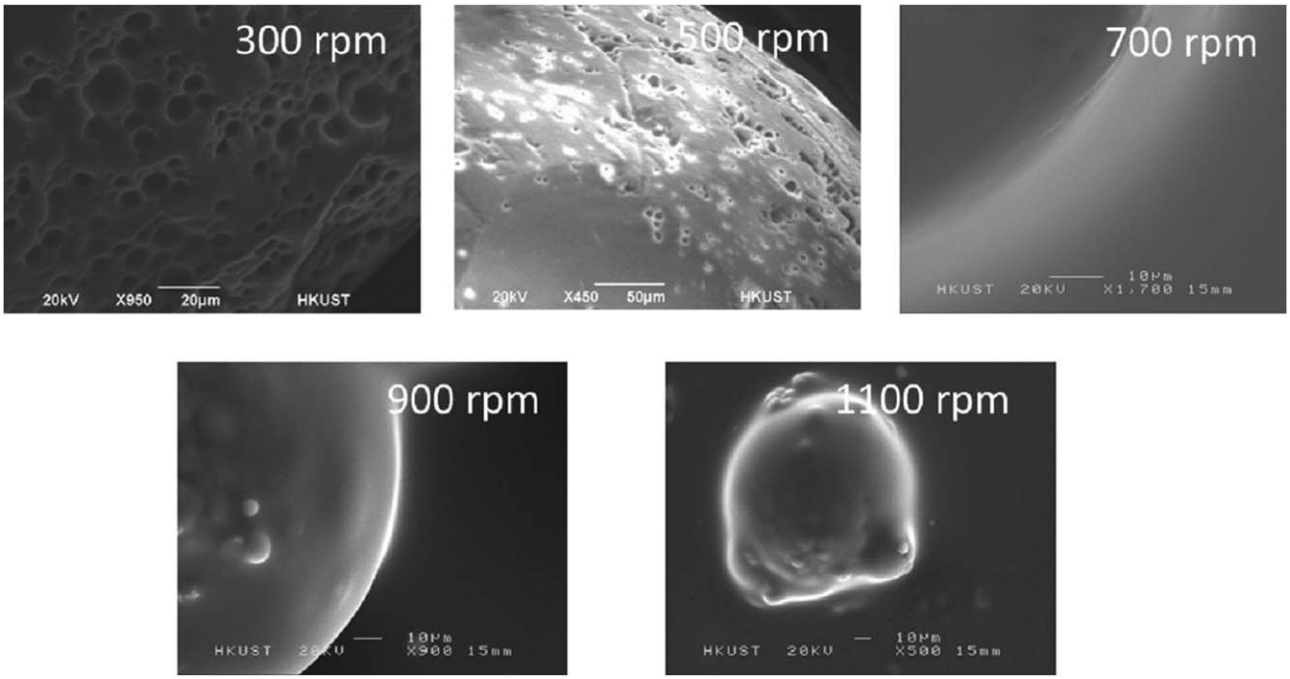

Figure 4. SEM images of silica-based microcapsules synthesized at different polymerization speeds.

From this result, it can best be concluded that the optimum monomer condition should be 15% by weight of monomer.

Characterization of Self-Healing Microcapsules

Silica-based microcapsules produced using the optimized conditions (emulsification speed: 500 rpm; polymerization speed: 900 rpm; 15 wt % MDI) are shown in Figure 6. The silica sol microcapsules produced have an average size of 87 μm [Figure 6(a)] with a uniform shape and size. A further examination was performed in a single microcapsule [Figure 6(b)], which shows the silica particles inside the microcapsule. An inset SEM image shows the cross-sectional view of the microcapsule, exposing the silica core content with the shell layer encapsulating the core silica sol material. Figure 6(c) further illustrates the core–

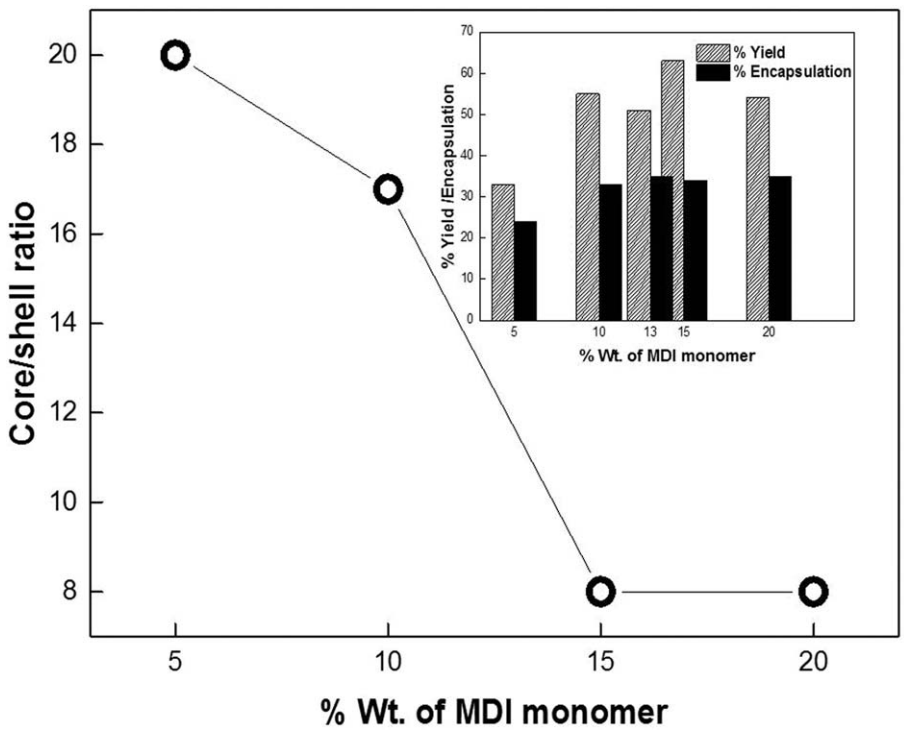

Figure 5. Effect of MDI monomer ratio on the core-shell ratio of microcapsules.

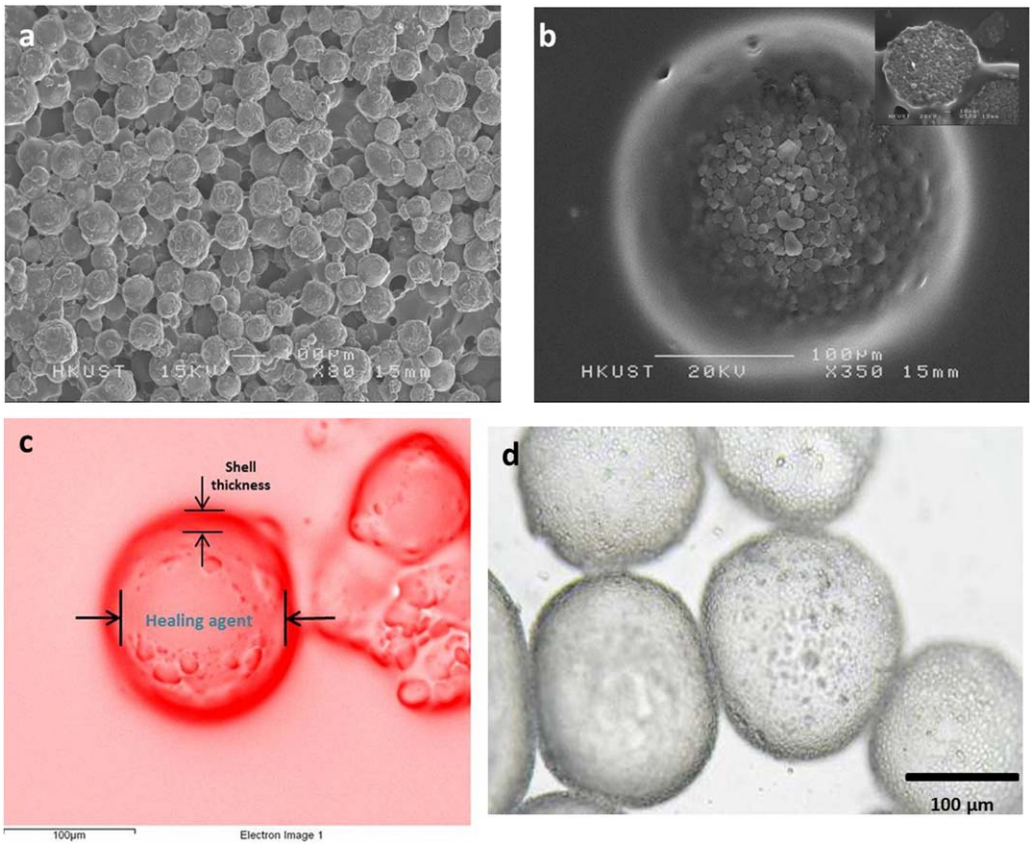

Figure 6. (a) SEM image of silica-based microcapsules, (b) SEM of a single microcapsule (inset is a cross-sectional view), (c) core-shell structure of the microcapsule, (d) optical image of microcapsules. [Color figure can be viewed in the online issue, which is available at wileyonlinelibrary.com.]

shell structure of the microcapsule, wherein a lighter shade of the capsule comprises the core materials, while the dark portion is of the polymeric shell, poly(urea-urethane). The optical image of the microcapsule [Figure 6(d)] shows how it behaves in solution and further shows the encapsulation of silica sol within its shell.

The FTIR spectrum in the transmittance mode of the silica-based microcapsules is shown in Figure 7. The appearance of the peak at 1705–1730 cm^{-1} represents the carbonyl of the free and bonded urethane groups, and peaks at 1660–1690 cm^{-1} represent the carbonyl of urea groups.[22] Furthermore, N—H stretching at 3300–3450 cm^{-1} and C—H asymmetrical at 2920 cm^{-1} also provide signatures for polyurethane groups. Silicon dioxide groups are represented by triple peaks: bending at 472 cm^{-1}, stretching at 803 cm^{-1}, and vibration at 1100 cm^{-1}.[36] Therefore, the microcapsule is composed of both the silica core and the polymeric shell of poly(urea-urethane).

Figure 8 displays the load-displacement curve of a silica-based microcapsule. An increasing load on the microcapsule was performed at a depth of 11,000 nm, held, and released at 16,500 nm. The nonlinear behavior of the loading portion of the curve indicates both elastic and plastic deformation,[37,38] and the shell shows an elastic displacement recovery during unloading. Similar results were observed in the work of Su *et al.*,[39] wherein the deformation load was more than 10 mN. This was attributed to the different molecular weight of the shell and its microstructure, such as thickness, density, and porosity. The force-displacement relationship in three stages is shown in Figure 8. First is the loading stage, wherein force increases with the depth of the microcapsule until it reaches its maximum load (140 mN), where force became constant at a certain holding time (second stage). The third stage is the sudden fall of the

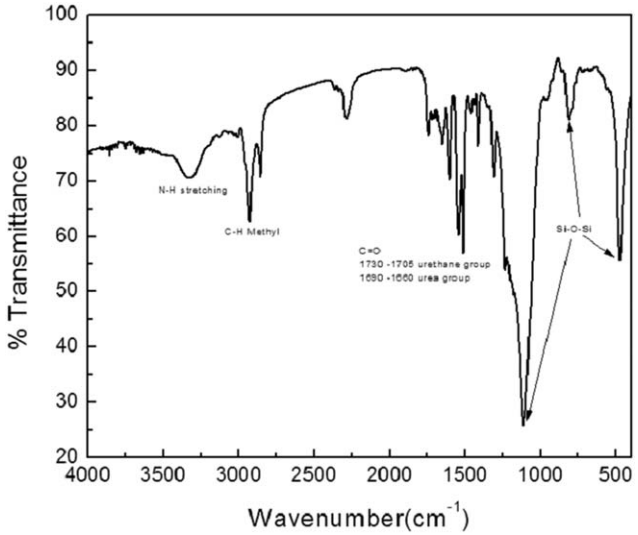

Figure 7. FTIR spectra of silica-based microcapsules.

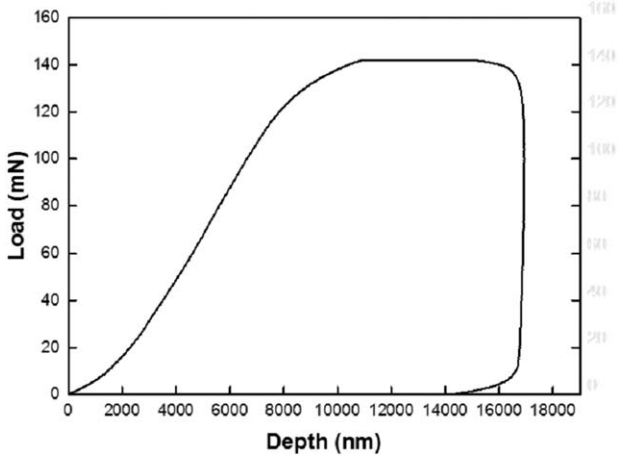

Figure 8. Load-displacement curve of silica-based self-healing microcapsules.

load at a certain depth of the microcapsule, indicating the rupture of the microcapsule and indicating its ultimate strength.

The polymeric shell material [poly(urea-urethane)] was further analyzed to investigate its mechanical properties. The analysis was carried out in a dynamic mechanical analyzer (DMA 7, Perkin Elmer), whereby tensile stress was applied on a poly(urea-urethane) film sample, and a stress–strain diagram was derived (Figure 9). Figure 9 demonstrates both the elastic and plastic properties of the poly(urea-urethane) film that is used as a polymeric shell layer of the self-healing microcapsules. The elastic property of the film is depicted on the linear curve exhibited on the figure. This shows that the film, at a certain load or stress range, is proportional to the elongation or strain it experiences. However, at a specific point or load, stress becomes constant while strain increases. This behavior shows the plastic property of the poly(urea-urethane) film.

To further analyze the stress–strain diagram of poly(urea-urethane) film, Figure 9 demonstrates how the mechanical properties such as elasticity, yield strength, and ultimate strength are derived. For example, the elasticity modulus is derived from the slope of the linear curve 1 [Figure 9 inset (a)]. This curve has a slope of 1300 Pa, which corresponds to the elasticity modulus value. In the same figure, inset (b), an offset linear curve is drawn to the right of curve 1. This new curve derives the yield strength of 29 kPa. Also, inset (c) shows a linear curve from the peak of the original plot representing the ultimate strength curve. The ultimate strength is derived from the peak point of the stress–strain curve. It has a value of 98 kPa.

Potential Application of Self-Healing Microcapsules in Concrete

The potential application of the synthesized self-healing microcapsules was demonstrated by analyzing the compressive and flexural strengths and water absorption in both normal and self-healing concrete samples. In this study, self-healing is evident in the improvement of the physical properties of the concrete, such as compressive and flexural strength and water absorption. Figure 10 shows the normalized compressive strength of both normal and self-healing concrete versus its conditions. This figure indicates that at the same initial compressive strength of both normal and self-healing concrete, both samples decreased their original strength after cracking. At this point, both strengths are almost the same. However, after submerging them into the water, healing was evident in the self-healing concrete by its increased strength. For the normal

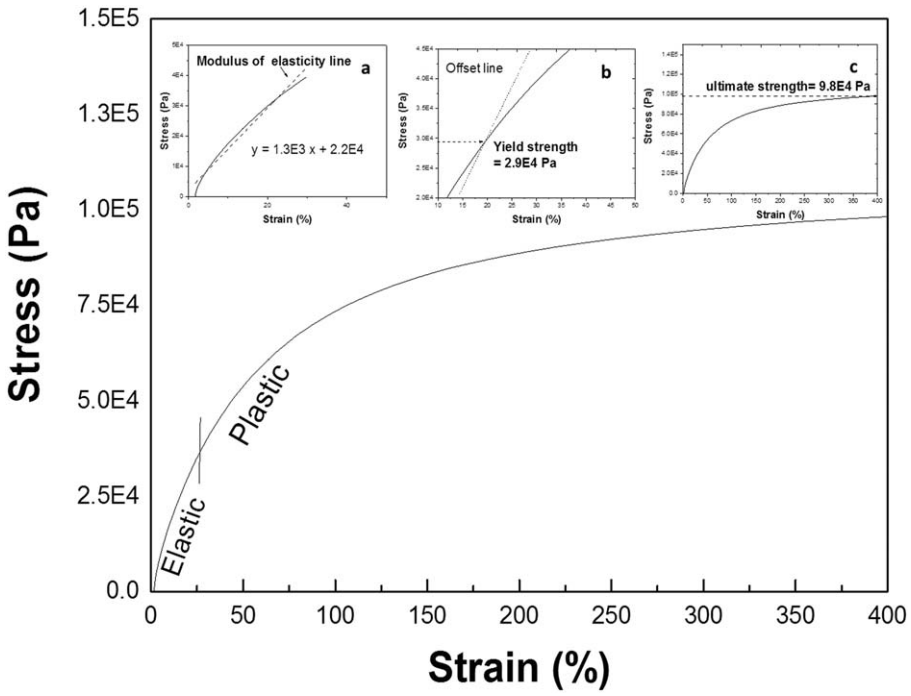

Figure 9. Stress–strain diagram for poly(urea-urethane) film used as a polymeric shell in silica-based microcapsules. Insets are figures that derive (a) elasticity modulus, (b) yield strength, and (c) ultimate strength.

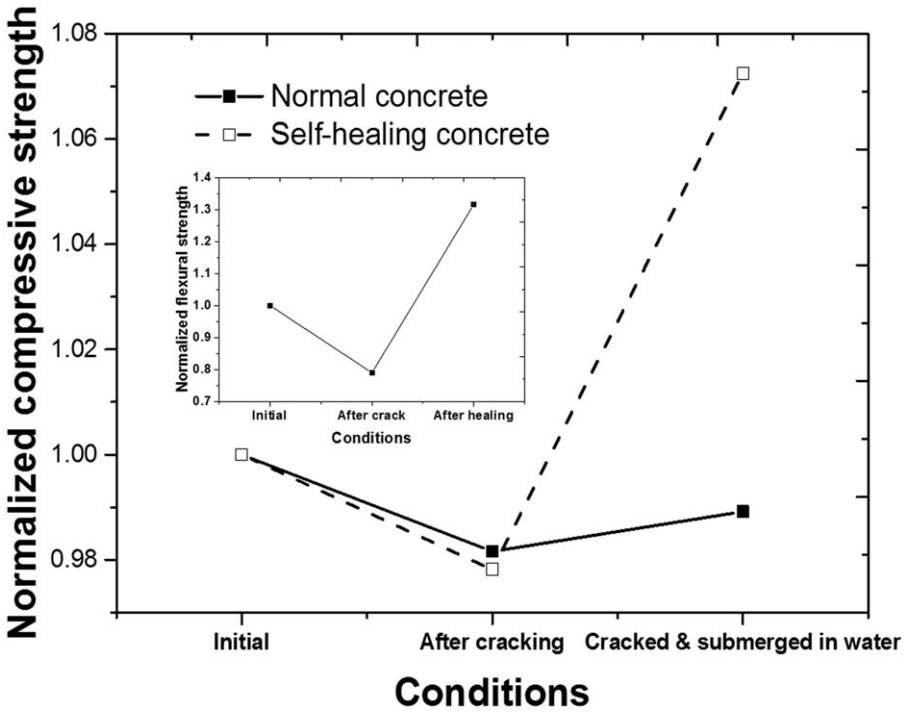

Figure 10. Normalized compressive strength of both normal and self-healing concrete at different conditions. Inset is the normalized flexural strength of self-healing concrete.

concrete, the increase of the compressive strength is very minimal and even less than its original. The same behavior was also observed in the normalized flexural strength of self-healing concrete, wherein after cracking the sample and submerging it in water, its flexural strength increased to greater than its original. This behavior demonstrates the self-healing ability of microcapsules in concrete. It is obvious in this case that mechanical loading induced strain on the concrete. Once the stress exceeded the concrete's strength capacity, cracking occurred. Concrete as a composite of aggregate and cement paste has a unique response to its applied load. Applied stress on pure cement aggregate and cement paste has a direct effect on its strain. However, for a composite such as concrete, it is nonlinear. This nonlinear behavior is caused by the development of microcracks,[40] which can be attributed to the weak bond or interfacial transition zone between the aggregate and the paste matrix.[41,42] Unreinforced concrete typically develops microcracks upon loading.[43,44] However, they are undetectable or have negligible effect on its load-displacement response. Consequently, these undetectable and propagating cracks can trigger microcapsules to break. A healing agent from the microcapsules, silica sols, are then released, which react with the calcium hydroxide from cement and produce a calcium silicate hydrate (C–S–H) gel that heals cracks. This mechanism is comparable to Pelletier *et al.*'s study.[22] However, instead of using sodium silicate, pure silica sol was used in this study. The use of such an amorphous form of silicate gives a more efficient formation of C–S–H gels and thus its healing properties to the concrete.

Another property of self-healing concrete is its ability to resist water absorption. Initial water absorption of self-healing concrete is 0.70%, and that of normal concrete is 1.7%. However, when both samples were subjected to microcracking, their water absorption was 0.70 and 3.53 for self-healing and normal concrete, respectively. This shows that self-healing concrete retains its initial value, which indicates that microcracking inside the sample was healed. A constant absorption result is consistent with the compressive strength result, in which after microcracking the strength is increased through the self-healing phenomenon. In contrast, normal concrete, when subjected to microcracking, creates more voids, which attract water. This results in a decrease in strength.

CONCLUSIONS

A self-healing microcapsule was successfully synthesized through a simple method and using a cheap alternative (silica sol) as a healing agent. The optimized conditions for the synthesis parameters (emulsification and polymerization speeds and monomer ratio) are helpful in obtaining the optimum size of the self-healing microcapsules. The optimized microcapsules are highly scalable, and that is a significant step for further commercialization. The application of self-healing microcapsules in concrete further verifies the self-healing phenomenon with an increase in compressive and flexural strengths after microcracking.

ACKNOWLEDGMENTS

The project is supported by the Innovation and Technology Fund, HKSAR Project (ITP/004/13NP), the Nano and Advanced Materials Institute (NAMI), Ltd., of Hong Kong, and The Hong Kong University of Science and Technology.

REFERENCES

1. White, S. R.; Sottos, N. R.; Geubelle, P. H.; Moore, J. S.; Kessler, M. R.; Sriram, S. R.; Brown, E. N.; Viswanathan, S. *Nature* **2001**, *409*, 794.
2. Garcia, S. J. In Smart Polymers and Their Applications; Woodhead Publishing Materials; Cambridge, UK, **2014**; Chapter 9.
3. Li, V. C.; Lim, Y. Y.; Chan, Y.-W. *Composites Part B* **1998**, *29B*, 819.
4. Pang, J. W. C.; Bond, I. P. *Compos. Sci. Technol.* **2005**, *65*, 1791.
5. Nishiwaki, T.; Mihashi, H; Hang, B.-K.; Miura, K. *J. Adv. Concr. Technol.* **2006**, *4*(2), 267.
6. Nosonovsky, M.; Amano, R.; Lucci, J. M.; Rohatgi, P. K. Phys. *Chem. Chem. Phys.* **2009**, *11*, 9530.
7. Tooher, K. S.; Sottos, N. R.; Lewis, A. L.; Moore, J. S.; White, S. R. *Nature Materials* **2007**, *6*, 581.
8. Wang, J.; Tittelboom, K. V.; Belie, N. D.; Verstrate, W. *Constr. Build. Mater.* **2012**, *26*, 532.
9. Bang, S. S.; Galinat, J. K.; Ramakrishnan, V. *Enzyme Microb. Technol.* **2001**, *28*, 404.
10. Jonkers, J. M.; Thijssen, A.; Muyzer, G.; Copuroglu, O.; Schlangen, E. *Ecol. Eng.* **2010**, *36*, 230.
11. Bang, S. S.; Galinat, J. K.; Ramakrishnan, V. *Enzyme Microb. Technol.* **2001**, *28*(4), 404.
12. Luhar, S.; Gourav, S. *Journal of Civil Engineering Research* **2015**, *5*(3), 53.
13. Tittelboom, K. V.; Belie, N. D.; Muynk, W. D.; Verstraete, W. *Cem. Concr. Res.* **2010**, *40*, 157.
14. Rodriquez-Navarro, C.; Rodriquez-Gallego, M.; Chekroun, K. B.; Gonzales-Munoz, M. T. *Appl. Environ. Microbiol.* **2003**, *69*(4), 2182.
15. Ghosh, P.; Mandal, S.; Chattopadhyay, B. D.; Pal, S. *Cem. Concr. Res.* **2005**, *35*, 1980.
16. Henk, M. J.; Arjan, T.; Gerard, M.; Oguzhan, C.; Erik, S. *Ecol. Eng.* **2008**, *36*, 230.
17. Talaiekhozan, A.; Keyvanfar, A.; Shafaghat, A.; Andalib, R.; Abd Majid, M. Z.; Ali Fulazzaky, M.; Mohamad ZIn, R.; Lee, C. T.; Hussin, M. W.; Hamzah, N.; Marwar, N. F.; Haidar, H. I. *Environ. Treat. Tech.* **2015**, *2*(1), 1.
18. Kessler, M. R.; Sottos, N. R.; White, S. R. *Composites Part A* **2003**, *34*, 743.
19. Hu, J.; Chen, H.-Q.; Zhang, Z. *Mater. Chem. Phys.* **2009**, *118*, 63.
20. Li, Q.; Mishra, A. K.; Kim, N. H.; Kulia, T.; Lau, K.-T.; Lee, H. *Composites Part B* **2013**, *49*, 6.
21. Huang, H.; Ye, G.; Sui, Z. *Constr. Build. Mater.* **2014**, *63*, 108.
22. Pelletier, M. M.; Brown, R.; Shukla, A.; Brose, A. Self-healing concrete with a microencapsulated healing agent; http://energetics.chm.uri.edu/system/files/Self%20healing%20concrete%20-7-11.pdf (accessed August 2013).
23. Kendrick, D. A.; Parsonage, J. R.; Vazifdar, R. V. *Cem. Concr. Res.* **1998**, *28*, 1537.
24. Baltakys, K.; Jauberthie, R.; Siauciunas, R.; Kaminskas, R. *Mater. Sci.–Poland* **2007**, *25*, 663.
25. Saihi, D.; Vroman, I.; Giraud, I.; Bourbigot, S. *React. Funct. Polym.* **2006**, *66*, 1118.
26. Keung, L. H.; Tan, N. P. B.; Choi, W. H.; Lam, W. C. Self-Healing Material and Preparation Process Thereof. U.S. Pat. Application 14/723477.
27. Griffin, W. C. *J. Soc. Cosmet. Chem.* **1949**, *1*, 372.
28. Lyman, D. L. Polyurethanes. The Chemistry of the Diisocyanate-diol Reaction; Marcel Dekker: New York, **1972**.
29. Pense, A. M.; Vauthier, C.; Benoit, J. P. *Colloid Polym. Sci.* **1994**, *272*, 211.
30. Salaun, F.; Bedek, G.; Devaux, E.; Dupont, D.; Gengembre, F. *J. Membrane Sci.* **2011**, *370*, 23.
31. Hong, K.; Park, S. *React. Funct. Polym.* **1997**, *42*, 193.
32. Lukaszczy, J.; Urbas, P. *React. Funct. Polym.* **1997**, *33*, 233.
33. Brown, E. N.; Kessler, M. R.; Sottos, N. R.; White, S. R. *J. Microencapsulation* **2003**, *20*, 719.
34. Rallison, J. M. *Annu. Rev. Fluid Mech.* **1984**, *16*, 45.
35. Yang, J.; Keller, M. W.; Moore, J. S.; Sotto, S. R.; Sottos, N. R. *Macromolecules* **2008**, *41*, 9650.
36. Zhang, W. H.; Fan, X. D.; Tian, W.; Fan, W. W. *eXPRESS Polym. Lett.* **2012**, *6*, 532.
37. Tehrani, M.; Safdari, M.; Al-Haik, M. S. *Int. J. Plast.* **2010**, *27*, 887.
38. Seltzer, R.; Mai, Y.-W. *Eng. Fract. Mech.* **2008**, *75*, 4852.
39. Su, J.-F.; Wang, X.-Y.; Dong, H. *Mater. Lett.* **2012**, *89*, 1.
40. Hsu, T. T. C.; Slate, F. O.; Struman, G. M.; Winter, G. *J. Am. Concr. Inst.* **1963**, *60*, 209.
41. Mehta, P. K. In Durability of Concrete, ACI SP-126; Malhotra, V. M., Ed.; American Concrete Institute: Farmington Hills: MI, **1993**; p 1.
42. Shah, S. P.; Slate, F. O. International Conference on the Structure of Concrete. A. E. Brooks and K. Newman, Ed., Imperial College: London, **1965**; p 1.
43. Atiogbe, E. K.; Darwin, D. *ACI Mater. J.* **1987**, *84*(6), 491.
44. Li, Z.; Kulkarni, K.; Shah, S. P. *Exp. Mech.* **1993**, *33*, 181.
45. Zhu, D. Y.; Rong, M. Z.; Zhang, M. Q. *Prog. Polym. Sci.* **2015** http://dx.doi.org/10.1016/j.progpolymsci.2015.07.02 (accessed 25 September 2015).
46. Hong Kong Observatory, Climate Change, Observed Climate Change in Hong Kong, Rainfall; http://www.weather.gov.hk/climate_change/obs_hk_rainfall_e.htm (accessed October 2015).
47. Moisture in Concrete and Moisture-Sensitive Finishes and Coatings, Data Sheet; Cement Concrete & Aggregates Australia: Mascot NSW, Australia; April **2007**.